CHEMISTRY
AN ASIAN JOURNAL
www.chemasianj.org

Accepted Article

Title: Motion Induced Change in Emission as an Effective Strategy for Ratiometric Probing of Human Serum Albumin and Trypsin in Biological Fluids

Authors: Nilanjan Dey, Basudeb Maji, and Santanu Bhattacharya

To be cited as: *Chem. Asian J.* 10.1002/asia.201701795

Link to VoR: http://dx.doi.org/10.1002/asia.201701795

A Journal of

ACES
Asian Chemical Editorial Society

A sister journal of **Angewandte Chemie** and **Chemistry – A European Journal**

WILEY-VCH

10.1002/asia.201701795

WILEY-VCH

Motion Induced Change in Emission as an Effective Strategy for Ratiometric Probing of Human Serum Albumin and Trypsin in Biological Fluids

Nilanjan Dey,[a] Basudeb Maji[a] and Santanu Bhattacharya*[a], [b]

Abstract: We report a highly luminescent pH sensitive, thermo-reversible nanoaggregate material in pure aqueous medium via self-agglomeration of carbazole-based amphiphiles. The self-assembly process restricts the intramolecular motions of the molecules and induces a change in emission signal from blue to cyan (AIE effect). A similar kind of ratiometric response is also observed in presence of human serum albumin (HSA). However, here the molecular motion of the flexible fluorescnce probe is restricted by its embdding microenvironment, not aggregation (MICE effect). Moreover, the probe shows fairly high selectivity towards HSA over other serum albumin proteins. Our carbazole-based fluorescence probes are a unique example, where ratiometric sensing of HSA is achieved solely by involving reversible noncovalent interactions. Considering the high significance of HSA in clinical diagnosis, a wide range of biological fluids, such as human urine, saliva, and plasma have been screened for analyzing HSA contents. In addition to this, the present system is employed for detection of trypsin at sub-nanomolar concentration via digestion of HSA.

Introduction

Human Serum Albumin (HSA), the most abundant plasma protein present in our circulatory system, plays a pivotal role in maintaining plasma osmotic pressure and also transporting a wide range of exogenous as well as endogenous biomolecules.[1,2] The abnormal level of HSA in human body is the symptom of many diseases, such as hepatitis, liver cirrhosis, diabetes mellitus *etc*.[3,4] Thus quantification of albumin level in biological fluids (blood serum, urine, saliva etc.) can serve as a major diagnostic test for the patients suffering from the above-mentioned illness.[5-8] There are three different sensing strategies known in the literature for the estimation of serum albumins, such as dye-binding based optical assay, antibody-based immunochemical method, and the LC-MS/MS-based proteomic technique.[9-12] Among all these strategies, the colorimetric assay is the most user-friendly one, since it is cost-effective and less tedious with the minimum number of sample preparation steps.[13-18] The clinically approved optical methods mostly involve Bromocresol green (BCG) as the color generating dye.[19] Though the high sensitivity of BCG towards HSA can be beneficial for the estimation purpose, it can interact with other plasma proteins within the 30s of incubation leads to the overestimation of albumin level.[20,21] Thus this time-sensitive nature can restrict the applicability of this probe in developing high throughput quantification assay. On the other hand, recently, fluorogenic probes with aggregation-induced emission enhancement (AIEE) property have become immensely popular in biomolecular sensing.[22] Presence of intramolecular rotating units makes these probes poorly emissive in the dispersed state (non-radiative decay). However, aggregation can restrict these intramolecular motions and reduce the number of non-radiative decay pathways.[23] Thus instead of getting conventional aggregation-induced emission quenching (AIEQ), aggregation-induced emission enhancement (AIEE) can be observed. Though there are several small molecules based AIEE sensors reported in the literature for selective detection of albumins, very few of them found to be suitable for actual clinical applications due to limited sensitivity (detection limit >30 μg/mL).[24] Moreover, discrimination among different kinds of serum albumin is very difficult utilizing optical sensors, since all of them posses highly resembled primary structures. Till date, only a handful of sensors have appeared in the literature, which could exhibit preferential interaction with HSA over its structurally homologous analog BSA.[25-29] Therefore careful consideration of these aforementioned points is essential to develop proper prognostic marker of HSA in biological fluids.

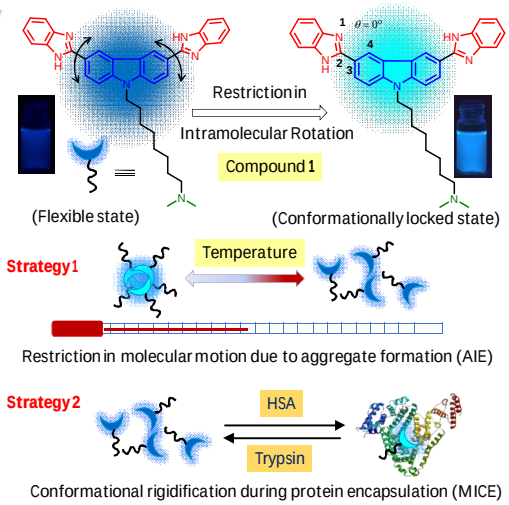

Figure 1. Structure of compound **1** with a schematic diagram showing its stimuli-responsive emission switching behavior [formation of highly emissive conformationally restricted state as a result of AIE (top) and MICE (below) effect].

Considering the present scenario, herein we have synthesized a series of easily synthesizable carbazole-based luminescent probes (Figure 1), which can form self-assembled luminescent nanoaggregates in water with high thermo-reversibility and pH sensitivity. The compound **1** exhibited highly selective ratiometric response towards (change in emission color from

[a] N. Dey B. Maji and Prof. S. Bhattacharya
Department of Organic Chemistry
Indian Institute of Science
Bangalore-560012
Email: sb@orgchem.iisc.ernet.in
[b] Present Address: Indian Association of Cultivation of Science,
Kolkata 700032, India

blue to cyan) HSA. Thus it can be considered as a unique example of ratiometric sensing of HSA through reversible noncovalent interactions. It is important to note that the ratiometric sensors are often superior to the 'turn-on' probes since they can provide an inbuilt correction to eliminate interferences caused by the sudden change in the external environment. Further, the high specificity of the probes towards HSA was exploited to estimate albumin content in various biological fluids, such as human urine, saliva, and blood plasma samples. Finally, protease-induced hydrolysis of HSA was employed as an alternative strategy for identification of trypsin at physiological condition (pH 7.4).

Results and Discussion

Nanoaggregates formation of compound 1 at pH 6.0 in water

In non-polar solvent like THF, the fluorescence spectrum of compound **1** showed a moderately emissive band at ~400 nm, which experienced a strong red-shift (~70 nm) in Tris-HCl buffer (at pH 6.0) due to the formation of close-contact aggregates (Figure 2a). To validate the possible self-assembly processes of compound **1** at pH 6.0, detailed morphological transformations were investigated alongside with dynamic light scattering studies (Figure S1). The time-dependent emission studies indicated that in pure THF, compound followed single-exponential decay presumably due to the presence of uniformly-dispersed monomeric units. However, the formation of long-lived excited state species with multi-exponential decay channel was observed at pH 6.0 (Figure 2b & S2). In dispersed state, the probe molecules experience high conformational flexibility, which enhances the possibility of non-radiative relaxation (smaller decay constant/ faster decay). On the contrary, in aggregated state the intramolecular motions becomes restricted, which stabilizes the excited state in greater extent (higher decay constant/ slower decay).[30] The temperature variation studies suggested that the aggregation phenomenon was highly thermo-reversible in nature, even up to multiple numbers of the cycle. A clear shift from aggregate to monomer emission was observed when the temperature was raised from 15 to 85 °C (Figure 2c & S3). Reversal of solution temperature back to 15 °C, regenerated the aggregate emission band. Changes in pH of the medium indicated that the maximum inter-chromophore association was observed at pH range 4.5–6.5 due to protonation at the benzimidazole sites (Figure S4). Also, the addition of conventional assembly–promoting electrolytes, such as KCl was found to escalate the agglomeration process (Figure S5).[31] When emission spectrum of **1** was recorded in a highly viscous medium (30% glycerol in water), a similar type of emission enhancement was observed at 454 nm band due to restricted motions of the individual interactive units (Motion-induced change in emission) (Figure 2d). From the above shred of observations, we can conclude that the red-shifted emission band in case of nanoassembly also arises as the moleucles adopt rigid molecular structure in the aggregated state (AIE effect).[32] The stimuli-response nature of the aggregates will also allow utilizing these probes for diverse biomedical applications, such as drug delivery or sensing.[33-36]

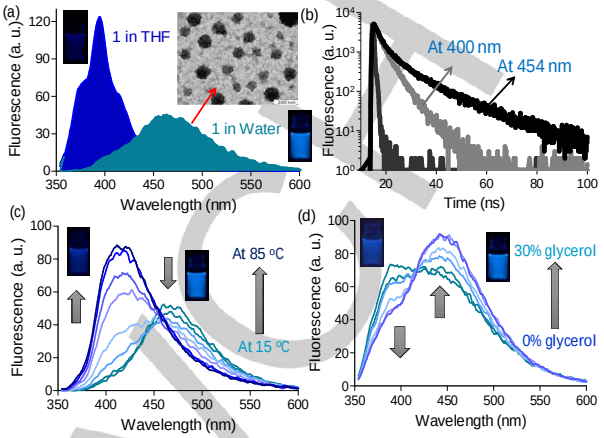

Figure 2. (a) Emission spectrum of **1** (λ_{ex} = 350 nm, 10 μM) both in THF and in PBS buffer at pH 6.0 [Inset shows TEM images of **1**]. (b) Time-dependent emission decay of **1** at 400 and 454 nm at pH 6.0 in water (λ_{ex} = 350 nm, 10 μM). (c) Temperature-dependent changes in emission spectra of **1** (λ_{ex} = 350 nm, 10 μM) at pH 6.0 in PBS. (d) Emission spectra of **1** (λ_{ex} = 350 nm, 10 μM) in different glycerol-water mixture media (0-30% glycerol) at pH 6.0, 37 °C.

Interaction of compounds with plasma proteins at pH 7.4

After demonstrating the molecular dynamic controlled two distinct photophysical properties of the probe **1**, we sought to exploit its molecular recognition property. Thus we proceeded to investigate its interaction with serum albumins since these macromolecular hosts are known to induce conformational rigidification in the amphiphilic guest molecules upon encapsulation. To eliminate the influence of temperature and pH on the sensing stuides, we fixed the pH of the medium as 7.4 and temperature at 37 °C for all the subsequent studies. Though the compound showed monomeric emission (λ_{em} = 400 nm) at this condition due to the presence of uniformly dispersed building units, an addition of human serum albumin (HSA) could rapidly change the emission color from blue to cyan by producing a red-shifted emission band at 454 nm. However, no shift in emission maxima was observed when the compound was allowed to interact with other non-targeted enzymes and proteins (Figure 3a). Further, the selectivity of **1** towards HSA was investigated in presence of various biologically relevant ionic analytes, neutral compounds, and thiol-containing amino acids. As shown in Fig. S6, only HSA could elicit a dramatic increase in the fluorescence intensity at 454 nm, while other analytes led to negligible changes in fluorescence intensity (Figure S6). Concentration-dependent emission studies with HSA indicated that at a lower concentration of HSA (0-25 mg/L), emission quenching was observed at 400 nm band, while at high concentration (30-80 mg/L), fluorescence enhancement was noticed at 454 nm (Figure 3b). Thus we could observe a dose-dependent linear change in the emission intensity over a wide range of HSA concentration (0-80 mg/L) (Figure 3c). This linear ratiometric response is very crucial for accurate estimations of HSA level in unknown samples with minimum background interference. Further, the limit of detection (using blank variation

method) of **1** for HSA in PBS (pH 7.4 at 25 °C) was determined to be 0.27 mg L^{-1}.[37-39]

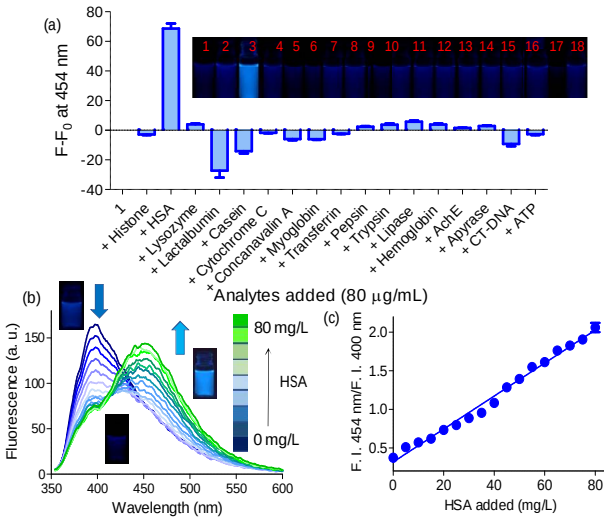

Figure 3. (a) Changes in emission intensity of **1** (λ_{ex} = 350 nm, 10 μM) at 454 nm in presence of various bio-analytes at pH 7.4 (Images show changes in emission color of **1** in presence of analytes, the sequence is same as mentioned in the bar plot). (b) Emission titration of **1** (λ_{ex} = 350 nm, 10 μM) with HSA (0–80 mg/L) at pH 7.4 in PBS buffer. (c) Ratiometric change in emission intensity of **1** (λ_{ex} = 350 nm, 10 μM) upon addition of HSA at pH 7.4 PBS buffer.

The analysis of thermodynamic parameters (ΔH and ΔS) as calculated from variable temperature emission titration studies indicated that compound **1** with HSA involves a combinational effect of electrostatic and hydrophobic interactions (Table S1).[40] A negative value of ΔH with positive entropy change (ΔS) at 400 nm, suggested that the spectral changes at 400 nm were governed by the electrostatic interactions. At the same time, positive changes in both enthalpy and entropy values were observed at 454 nm, which ensured the role of hydrophobic interaction in the recognition process.[41-43] From the above observations, it can be assumed that there may be two independent binding sites available for compound **1** in HSA. Some molecules (due to the positively charged backbone) will nonspecifically bind to the negatively charged surface of the protein via electrostatic interaction, mostly with surface-exposed negatively charged functional groups, like carboxylates or hydroxyl groups *etc*. Since the surface exposed negatively charge in case of HSA will be pH dependent, the extent of quenching (at 400 nm) will also be affected by pH of the medium. Since electrostatic complexation can enhance the micropolarity around the probe molecules, an emission quenching is observed due to dipole-dipole interaction. It is important to note that quenching of emission intensity at 400 nm was also observed in presence of other proteins we well, especially upon addition of proteins with pI value < 6.0, such as casein, α-lactalbumin etc (Figure S7). This confirmed the nonspecific nature of the electrostatic interaction. On the other hand, owing to their amphiphilic nature, some of the probe molecules may go inside the hydrophobic interior of the HSA (highly selective for HSA as observed in figure 3a). This may significantly alter the motions of the embedded molecule (from flexible to restricted motion) and a 'turn-on' emission signal can be observed at 454 nm band (Figure 4 & S8, Scheme S1).[44,45] Though the excited state properties (increase in fluorescence intensity at 454 nm) of FONs of **1** (formed at pH 6.0) is quite similar to that of **1** + HSA complex, their ground state characteristics are entirely different. In the former case, intramolecular motions of the monomer units become in molecular aggregates (AIE effect), whereas in the later situation, the single probe experiences motion changes upon complexation with an analyte, here HSA (MICE effect). In spite of striking similarity in the output emission signal, no aggregate formation was observed in the presence of HSA.

As the albumins from different species mostly possess highly homologous primary structure, differentiation among them is difficult.[46] However, when emission spectra of **1** were recorded in presence of other serum albumins (like HSA, BSA, RSA *etc.*), comparatively larger emission enhancement was observed with HSA at 454 nm band (Figure 5a). However, no such preference was witnessed when changes in emission intensity of **1** were recorded at 400 nm band (Figure S9). This might be expected, as at 400 nm, the emission response mostly dominated by the nonspecific electrostatic interaction. Surfactants can destroy the native structure of albumin protein and preferentially bind to its hydrophobic pockets (exposed during denaturation).[47,48] Thus, when the emission response of **1** towards HSA was monitored in presence of CTAB, no red-shifted emission band could be observed (Figure S10). This again indicated the red-shifted emission band at 454 nm appeared during the encapsulation of dye molecules inside hydrophobic pockets of the protein. However, there was barely any change in the extent of emission quenching at 400 nm band.

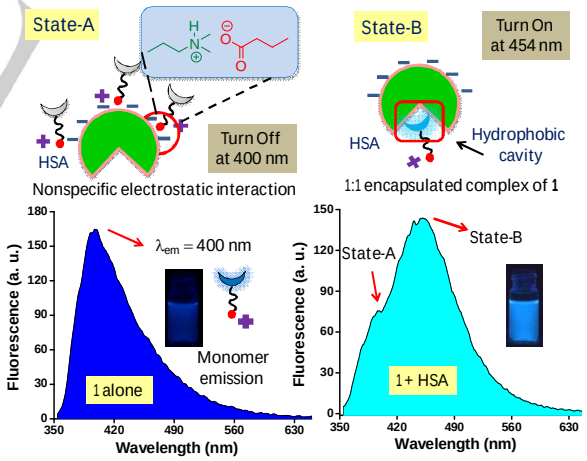

Figure 4. A schematic diagram shows two different modes of interaction of **1** with HSA at pH 7.4, nonspecific electrostatic interaction (State A) and site-specific hydrophobic encapsulation (State B).

The identification of the binding site (site of encapsulation) of **1** in HSA is very crucial for a deep understanding of its working principle. In order to do so, we first determined the stoichiometry of interaction of **1** with protein at 454 nm band using continuous variation method.[49,50] An inflection point at ~0.5 mol-fraction suggested there might be a 1:1 interaction of **1** with HSA (Figure

S11). The site-specific nature of **1** was verified by conventional dye displacement assays in presence of three different albumin binding drugs, including warfarin (domain IIA), ibuprofen (domain IIIA), and digitoxin (domain IIIB) (Figure 5b).[51] The selective displacement of warfarin (~50-53 %) suggested that the dye might have a preference towards the site-IIA of HSA. The shallow binding pocket of HSA at domain IIA (in comparison to BSA) can explain the higher degree of RIR in case of HSA with expected larger emission enhancement at 454 nm band.[52] The time-dependent emission studies indicated an increase in average decay time of **1** in presence of HSA (Figure S12). This is quite expected, since in the encapsulated state, probe molecule adopts rather rigid molecular structure and thus fluorescence dominates the energy transfer process, not the non-radiative relaxation.[53,54] Along with conformational rigidity, the relatively hydrophobic environment around the dye molecules also diminishes the possibility of water-mediated emission quenching upon encapsulation.This was evident by the higher quantum yield (at 454 nm) of the dye in presence of HSA (Φ = 0.18) as compared to its nanoaggregate form (Φ = 0.1). Besides this, changes in circular dichroism signals of the protein upon incubated with different amount of **1** showed a perturbation in the α-helical structure of the protein template (Figure 5c). This suggested that the probe molecule is embedded in the α-helices from subdomain IIA of HSA.[55,56] The FT-IR analysis also revealed that FT-IR stretching frequencies (amide I band, -OH and –NH) related to α-helices of protein got affected during interaction with **1** (Figure S13 & S14).[57,58]

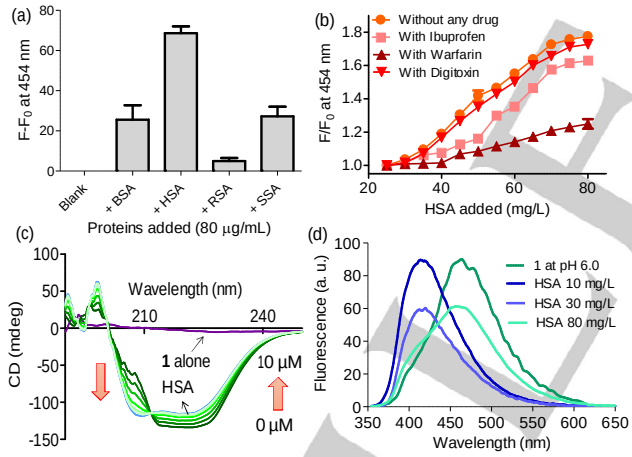

Figure 5. (a) Change in emission intensity of **1** (λ_{ex} = 350 nm, 10 μM) at 454 nm upon addition of different kinds of albumin at pH 7.4 in PBS buffer. (b) Drug-displacement assay of **1** (λ_{ex} = 350 nm, 10 μM) for identifying site-specific interaction of **1** with HSA at pH 7.4 in PBS. (c) Circular dichroism spectra of HSA (80 mg/L) in presence of **1** (0-10 μM) at pH 7.4. (d) Interaction of compound **1** (λ_{ex} = 350 nm, 10 μM) with HSA at pH 6.0 in PBS buffer.

Effect of pH on the extent of HSA sensing

As the compound showed a prominent influence of pH on its assembly formation behavior, we investigated the effect of pH on its albumin sensing property. The emission spectrum of **1** at pH 6.0 clearly showed aggregate emission with a maximum at 454 nm. Titration with HSA at this condition induced dissociation of the preformed molecular self-assembly at lower concentration range (0-10 μg/mL), which was perceptible from the blue shift (~45 nm) in the emission maximum. Further increase in HSA concentration (10-90 μg/mL) showed a similar type of spectral change as observed at pH 7.4, *i.e.* first quenching of the emission intensity at 400 nm band as HSA concentration varied from 10-40 μg/mL (electrostatic interaction) and then a 'turn-on' emission response at 454 nm from 40 to 90 μg/mL (MICE effect) (Figure 5d & S15). However, the extent of emission quenching at 400 nm was found to be inferior in this case due to poor electrostatic binding of the dye molecules with HSA. The probable reason for this might be the lowering of surface-exposed negative charge of HSA due to pH-driven shift in the protonation equilibrium.

Effect of terminal functional groups on HSA sensing

To investigate the role of aliphatic chain and the end functional groups on the protein recognition ability of the probe, we involved additional compounds in studies with variation in the chain lengths (C_4 vs. C_8 aliphatic chain) and end-functional units (tertiary nitrogen ends vs. quaternary ammonium center) (Figure S16). Surprisingly, all these compounds showed prominent nano-assembly formation in water (at pH 6.0) despite their structural diversity (Figure S17). Variable temperature studies ensured the thermo-reversible nature of aggregates remained unfazed even after modifying the lengths of the aliphatic chain or the nature of the terminal functional group (Figure S18). Besides that, pH and ionic strength dependent changes in emission signals were also observed similar to that of compound **1** (Figure S19). However, interaction with HSA clearly indicated that the compounds having the hard positive charge at the nitrogen end (**2** and **4**) experienced stronger dipole-dipole interaction with the surface-exposed negatively charged functional groups of HSA. This led to a higher degree of emission quenching at 400 nm band in presence of HSA (higher Stern-Volmer quenching constant values) at pH 7.4 (Figure 6a & Table S2).

On the other hand, compounds with longer aliphatic chains (**1** and **2**) will have higher tendency to go into the hydrophobic cavity of the protein molecule (type 2 interaction). Thus a higher degree of emission enhancement (population of molecule bound to the hydrophobic cavity is more) could be observed at 454 nm (Figure 6b & Figure S20). Nevertheless, in all the cases, we could observe the distribution of compounds in both interactive sites. Thus irrespective of their extent of interaction, one can observe emission quenching at 400 nm and fluorescence turn-on at 454 nm band.

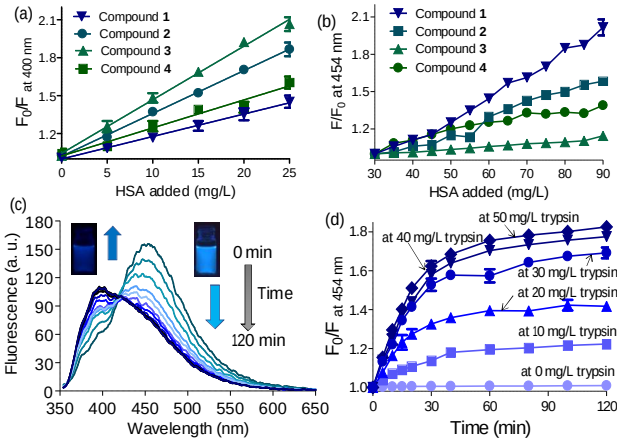

Figure 6. Change in emission intensities of compounds (**1-4**) upon addition of HSA (a) monitored at 400 nm, (b) monitored at 454 nm. (c) Time-dependent changes in emission spectra of **1** + HSA upon addition of trypsin (50 mg/L) in water (pH 7.4). (d) Time-dependent changes in emission intensity of **1** + HSA at 454 nm with various amounts of trypsin (0-50 mg/L).

Detection of Trypsin through digestion of HSA template

The design of optical probes for trypsin is highly desirable for clinical diagnosis purpose as its abnormal level in the human body could serve as the marker for many cardiovascular and neurodegenerative diseases.[59-61] Thus we asked if the preformed probe-HSA conjugate can be repurposed as the template for trypsin sensing. Even though trypsin does not directly interact with the probe molecule, trypsin-mediated digestion of protein should release the encapsulated probe molecule into the bulk medium. As a result, probe molecule can regain its conformational flexibility (change in motion from restricted to flexble). Thus the addition of trypsin could induce quenching in the emission intensity of **1** + HSA ensemble at 454 nm. A 2 h incubation time was needed to observe the saturation in the emission signal of **1** + HSA in presence of trypsin (Figure 6c). Further, time-dependent changes in the emission intensity of **1** + HSA (at 454 nm) were monitored at different trypsin concentrations, varied from 0 to 50 mg/L at pH 7.4 (Figure 6d).The minimum detectable concentration of trypsin was determined to be 0.15 mg/L. As biological matrices may contain other hydrolytic enzymes as well, we studied the sensitivity of the system against other enzymes, such as lipase, apyrase, glucosidase *etc*. To our relief, none of these enzymes produced detectable alternation in emission signal of **1** + HSA (Figure S21a). As EDTA is known for inhibiting the activity of trypsin at biological pH, we repeated the emission studies of **1** + HSA with trypsin in presence of 10 mM EDTA.[62] As expected, here we could observe the lesser extent of interaction with trypsin (Figure S21b).

Estimation of HSA in different biological fluids

The variation of HSA levels in human serum, urine or saliva can serve as the biomarker for various diseases. We exploited the rapid response of **1** towards HSA in estimating albumin contents of these complex biofluids. The normal concentration of a range of HSA in blood serum is 35–50 mg/L. However, its low level (hypoalbuminemia) indicates diseases like nephrosis, gastrointestinal protein loss, while high level (hyperalbuminemia) suggests dehydration and increase the body weight.[63-65] Similarly, the reference range of albumin in urine is 2.2–25 mg/L. Higher concentration of albumin in human urine normally suggests high permeability of renal glomeruli due to diabetes or renal damage.[66,67] On the other hand, the normal concentration of HSA in saliva is generally less than 0.5 g/L. An increase in concentration, in this case, indicates severe health problems such as type-2 diabetes mellitus or stomatitis *etc*.[68] In a typical experimental procedure, we have monitored the change in emission intensities of **1** both at 400 and 454 nm band in presence of serum/urine/saliva samples appropriately diluted in buffer medium (pH 7.4) (Figure 7a, c, e). The HSA concentrations in these matrices were then estimated using standard calibration plot as obtained from the titration studies in normal buffered medium (pH 7.4). To our relief, the HSA levels estimated by the present method were found to be close to the results determined by using the BCG method (Figure 7b, d, f). The relative variations between these two methods are less than 15% in all cases (Table S3-S5). Notably, the plasma, urine, and saliva samples need to be diluted by 50, 20 and 1000 fold respectively for the present assay, which means that only 4 µL of plasma, 10 µL of urine and 0.2 µL of saliva will be sufficient for HSA quantification by **1**. These findings suggested that quantification of HSA by this newly developed protocol was quite sensitive and highly reliable.

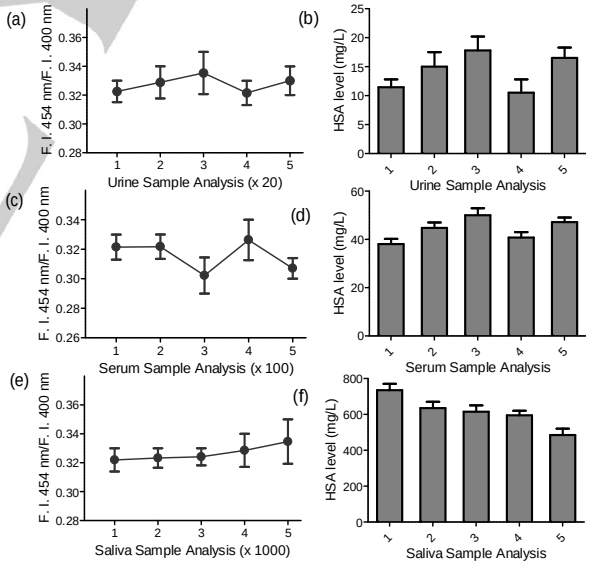

Figure 7. (a, c, e) Change in emission intensities of **1** (λ_{ex} = 350 nm, 10 µM) upon addition of diluted urine, serum and saliva extracts at pH 7.4 in water (b, d, f) Estimation of HSA contents of urine, serum and saliva samples collected from healthy individuals.

Conclusions

In summary, we have developed a series of rapidly scalable carbazole-based amphipathic dyes, capable of forming thermo-reversible, pH-sensitive nanoaggregates at pH 6.0 in water.

Though the compounds did not show any assembly formation at pH 7.4, they could exhibit a change in emission signal from blue to cyan upon binding to HSA. The mechanistic investigation suggested the distribution of compounds at two independent interaction sites. Nonspecific electrostatic binding of the compound onto the negatively charged protein surface led to 'turn-off' response at 400 nm band (blue emission, electrostatic effect), while encapsulation of dye into the hydrophobic cavity of site-IIA induced 'turn-on' response at 454 nm (cyan emission, MICE effect). Thus we could achieve ratiometric sensing of HSA solely by exploiting noncovalent interactions. Most notably, the probes also showed noticeably large interaction with HSA compared to other serum albumins, which makes them even more attractive for pathological applications. Further, quantification of HSA level was performed in a wide range of biofluids, including human urine, blood plasma, and saliva *etc*. In all cases, the estimated values were further verified by the well-established BCG method without notable variation (<15%). In addition, selective detection of trypsin (a digestive enzyme) was also achieved at a sub-nanomolar concentration by engaging preformed probe-HSA complex as the detection template. Thus we anticipate that the newly developed system can be converted into a diagonestic probe for ratiometric estimation of both HSA and trypsin in a wide range of biological fluids.

Experimental Section

Material and methods: All reagents and starting materials were obtained from the best known commercial sources and were used without further purification. Solvents were distilled and dried prior to use. FTIR spectra were recorded on a PerkinElmer FTIR Spectrum BX system. ^{1}H and ^{13}C NMR spectra were recorded on a Bruker Advance DRX 400 spectrometer operating at 400 and 100 MHz for ^{1}H and ^{13}C NMR spectroscopy, respectively.

Design and Synthesis of compounds 1-4: All the compounds involved in the present study were synthesized based on methods reported in the literature.[69,70] (Please see ESI)

UV-visible and fluorescence Experiment: The UV−vis and fluorescence spectra were recorded on a Shimadzu model 2100 UV-vis spectrometer and Cary Eclipse spectrofluorimeter respectively. In the emission experiments, the slit widths (for both the excitation and emission channel) and the excitation wavelengths were chosen based on the absorption maxima of the probe molecules. To monitored the effect of pH, sensing experiment was performed in buffered media of different pH (HCO_2Na/ HCl buffer for pH 2, Tris/HCl for pH 7 and $Na_2B_4O_7{\cdot}10H_2O$/NaOH for pH 12). Again during temperature-dependent experiments, 5 min of incubation was given in each case for thermal equilibrium.

Transmission Electron Microscopy (TEM): The samples were made under the dust-free condition and onto a Formvar-coated, 400 mesh copper grid and allowed to remain for 15 min. After that, the grid was air-dried and the last traces of solvent were removed under high vacuum. Then the changes in morphologies were observed under TEM (TECNAI T20) operating at an acceleration voltage (DC voltage) of 100 keV. Micrographs were recorded at a magnification of 10000-80000 X.

Dynamic Light Scattering Studies (DLS): DLS measurements were done using a Malvern Zetasizer NanoZS particle sizer (Malvern Instruments Inc., MA) instrument. Samples were prepared and examined under dust-free conditions. Mean hydrodynamic diameters reported were obtained from Gaussian analysis of the intensity-weighted particle size distributions.

Atomic Force Microscopy (AFM): Solutions of the samples were drop-cast on freshly cleaved mica sheets and then carefully air-dried 48 h. The AFM images of the samples were recorded using a JPK 00901 AFM instrument and analyzed using a Nano-Wizard software: Tapping mode, 10 nm tip radius, silicon tip, 292 kHz resonant frequency, 0.7-1 Hz scan speed, 256x256, and 512x512–pixels. Finally, the images were analyzed using Pico View 1.8.6 software.

Circular Dichroism (CD): All the CD spectra were recorded on a JASCO instrument, Model J-815-150S. Experiments were performed by purging dry N_2 gas continuously. Data were collected in a quartz cuvette of 1 mm path length.

Fluorescence Microscopy: Diluted solutions of the samples are drop-coated on pre-cleaned glass slides and left overnight for drying in a dust free environment and finally evacuated. The fluorescence microscopic image was taken on an Olympus IX-71 microscope.

Fluorescence Decay Experiment: Fluorescence lifetime values were measured by using a time-correlated single photon counting fluorimeter (Horiba Jobin Yvon). The system was excited with nano LED of Horiba - Jobin Yvon with a pulse duration of 1.2 ns. Average fluorescence lifetimes (τ_{av}) for the exponential iterative fitting were calculated from the decay times (τ_i) and the relative amplitudes (a_i) using the following relation (1).

$$\tau_{av}=(a_1\tau_1^2+a_2\tau_2^2+a_3\tau_3^2)/(a_1\tau_1+a_2\tau_2+a_3\tau_3) \quad (1)$$

Where a_1, a_2 and a_3 are the relative amplitudes and τ_1, τ_2, and τ_3 are the lifetime values, respectively. For data fitting, a DAS6 analysis software version 6.2 was used.[71,72]

Estimation of thermodynamic parameters during ligand-protein interaction: The binding constants are first determined at a different temperature. Then the values of ΔH^o and ΔS^o are calculated from the slope and intercept of the Van't Hoff plot (2) of ln K against 1/T. The Gibbs energy change ΔG^o is estimated according to Eq. (3).

$$\text{Ln } K = (-\Delta H^o/RT) + \Delta S^o/R \quad (2)$$

$$\Delta G^o = \Delta H^o - T\Delta S^o \quad (3)$$

According to Ross and Subramanian, a positive ΔH value is usually taken as typical evidence for hydrophobic interactions. Furthermore, specific electrostatic interactions between ionic species in aqueous solution are characterized by a positive value of ΔS and a negative ΔH value, whereas negative ΔH value and negative ΔS value changes arise from van der Waals forces and hydrogen bond formation.[73]

Analysis of human urine, saliva, and serum samples: Human blood serum, saliva or urine samples of healthy volunteers were collected from Indian Institute of Science (IISc) Health Centre with written consent from the donors. The samples were stored at -80ºC for future use. During the experiment, the samples were first kept at room temperature for 0.5 h and then tested without any pre-treatment except required dilution in PBS.

Acknowledgements

S.B. thanks, DST (J. C. Bose Fellowship) for the financial support of this work. N.D. and BM thanks IISc for research

associate fellowship and the Indian Association for the Cultivation of Science, Kolkata for the financial support of this work presented in this manuscript.

Keywords: Human Serum Albumin • Fluorescent Nanoaggregates • Ratiometric Sensing • Biological Fluids • Trypsin

1. M. Dockal, D. C. Carter, F. J. Ruker, *Biol. Chem.* **1999**, *274*, 29303-29310.
2. U. Kragh-Hansen, V. T. G. Chuang, M. Otagiri, *Biol. Pharm. Bull.* **2002**, *25*, 695-704.
3. K. Hoogenberg, W. J. Sluiter, R. P. Dullaart, *Acta Endocrinol*. **1993**, *129*, 151-157.
4. G. C. Viberti, R. J. Jarrett, U. Mahmud, R. D. Hill, A. Argyropoulos, H. Keen, *Lancet* **1982**, *319*, 1430-1432.
5. J. Rozga, T. Piatek, P. Malkowski, *Ann. Transplant*. **2013**, *18*, 205-217.
6. V. Arroyo, R. Garcia-Martinez, X. Salvatella, *J. Hepatol.* **2014**, *61*, 396-407.
7. F. Kratz, *J. Control. Release* **2008**, *132*, 171-183.
8. D. Gupta, C. G. Lis, *Nutr. J*. **2010**, *9*, 69.
9. M. C. Tu, Y. T. Chang, Y. T. Kang, H. Y. Chang, P. Chang, T. R. Yew, *Biosens. Bioelectron*. **2012**, *34*, 286.
10. D. Caballero, E. Martinez, J. Bausells, A. Errachid, J. Samitier, *Anal. Chim. Acta* **2012**, *720*, 43-48.
11. X. T. Chen, Y. Xiang, A. J. F. Tong, *Talanta* **2010**, *80*, 1952-1958.
12. X. H. Wang, X. Y. Walng, Y. Q. Wang, Z. J. Guo, *Chem. Commun*. **2011**, *47*, 8127-8129.
13. J. Min, J. W. Lee, Y. H. Ahn, Y. T. Chang, *J. Comb. Chem.* **2007**, *9,* 1079-1083.
14. H. Sun, J. Xiang, X. Zhang, H. Chen, Q. Yang, Q. Li, A. Guan, Q. Shang, Y. Tang, G. Xu, *Analyst* **2014**, *139*, 581-584.
15. S. E. Smith, J. M. Williams, S. Ando, K. Koide, *Anal. Chem.* **2014**, *86*, 2332-2336.
16. Z. Huang, H. Wang, W. Yang, *ACS Appl. Mater. Interfaces* **2015**, *7*, 8990-8998.
17. W. I. S. Galpothdeniy, S. Das, S. L. De Roy, B. P. Regmi, S. Hamdan, I. M. Warner, *RSC Adv*. **2014**, *4*, 17533-17540.
18. L. Peng, R. Wei, K. Li, Z. Zhou, P. Song, A. Tong, *Analyst* **2013**, *138*, 2068-2072.
19. B. T. Doumas, W. A. Watson, H. G. Biggs, *Clin. Chim. Acta* **1971**, *258*, 21-30.
20. C. Parikh, R. Yalavarthy, A. Gurevich, A. Robinson, I. Teitelbaum, *Renal Failure* **2003**, *25*, 787.
21. C. L. H. Snozek, A. K. Saenger, P. R. Greipp, S. C. Bryant, R. A. Kyle, S. V. Rajkumar, J. A. Katzmann, *Clin. Chem.* **2007**, *53*, 1099.
22. D. Ding, K. Li, B. Liu, B. Z. Tang, *Acc. Chem. Res.* **2013**, *46*, 2441-2453.
23. Y. Hong, J. W. Y. Lama, B. Z. Tang, *Chem. Commun*. **2009**, *0*, 4332-4353.
24. Y. R. Wang, L. Feng, L. Xu, Y. Li, D. D. Wang, J. Hou, K. Zhou, Q. Jin, G. B. Ge, J. N. Cui, L. Yang, *Chem. Commun*. **2016**, *52*, 6064-6067.
25. H. Sun, J. Xiang, X. Zhang, H. Chen, Q. Yang, Q. Li, A. Guan, Q. Shang, Y. Tang, G. Xu, *Analyst* **2014**, *139*, 581–584.
26. J. Fan, W. Sun, Z. Wang, X. Peng, Y. Li, J. Cao, *Chem. Commun*. **2014**, *50*, 9573-9576.
27. X. Fan, Q. He, S. Sun, H. Li, Y. Pei, Y. Xu, *Chem. Commun.* **2016**, *52*, 1178-1181.
28. Y. H. Ahn, J. S. Lee, Y. T. Chang, *J. Comb. Chem.* **2008**, *10*, 376-380.
29. J. Li, J. Wu, F. Cui, X. Zhao, Y. Li, Y. Lin, Y. Li, J. Hub, Y. Ju, *Sens. Actuators, B* **2017**, *243*, 831–837.
30. Y. Ren, J. W. Y. Lam, Y. Dong, B. Z. Tang, K. S. Wong, *J. Phys. Chem. B* **2005**, *109*, 1135-1140.
31. A. Stirpe, M. Pantusa, B. Rizzuti, L. Sportelli, R. Bartucci, R. Guzzi, *Int J Biol Macromol.* **2011**, *49*, 337-342.
32. D. Su, C. L. Teoh, L. Wang, X. Liu, Y. T. Chang, *Chem. Soc. Rev.,* **2017**, *46*, 4833-4844.
33. N. Dey, B. Maji, S. Bhattacharya, *Anal. Chem.* **2017**, DOI: 10.1021/acs.analchem.7b03520.
34. N. Dey, S. Bhattacharya, *Anal. Chem*. **2017**, *89*, 10376-10383.
35. N. Dey, S. Bhattacharya, *Chem. Commun.* **2017**, *53*, 5392-5395.
36. N. Dey, S. Bhattacharya, *Chem. Eur. J*. **2017**, *23*, 16547-16554.
37. N. Dey, A. Ali, S. Podder, S. Majumdar, D. Nandi, S. Bhattacharya, *Chem. Eur. J.* **2017**, *23*, 11891-11897.
38. N. Kumari, N. Dey, K. Kumar, S. Bhattacharya, *Chem. Asian J*. **2014**, *9*, 3174 – 3181.
39. N. Kumari, N. Dey, S. Jha, S. Bhattacharya, *ACS Appl. Mater. Interfaces* **2013**, *5*, 2438-2445.
40. N. Dey, S. Jha, S. Bhattacharya, *Analyst* **2017**, DOI: 10.1039/C7AN01058C.
41. T. Yamaguchi, E. Amano, S. Kamino, S. Umehara, C. Yanaihara, Y. Fujita, *Anal Sci.* **2005**, *21*, 1237-1240.
42. Z. Xu, W. Yang, C. Dong, *Bioorg. Med. Chem. Lett.* **2005**, *15*, 4091-4096.
43. A. Varlan, M. Hillebrand, *Molecules* **2010**, *15*, 3905-3919.
44. J. Li, J. Li, Y. Jiao, C. Dong, *Spectrochim. Acta Mol. Biomol. Spectrosc.* **2014**, *118*, 48-54.
45. L. Qi, Z. Lu, W. H. Lang, L. Guo, C. G. Ma, G. H. Sun, *New J. Chem.* **2015**, *39*, 9234-9241.
46. K. A. Majorek, P. J. Porebski, A. Dayal, M. D. Zimmerman, K. Jablonska, A. J. Stewart, M. Chruszcz, W. Minor, *Molecular Immunology* **2012**, *52*, 174-182.
47. N. Dey, S. Bhattacharya, *Chem. Rec*. **2016**, 16, 1934–1949.
48. P. Kundu, S. Ghosh, N. Chattopadhyay, *Phys. Chem. Chem. Phys*. **2015**, *17*, 17699-17709.
49. N. Dey, B. Bhagat, D. Cherukaraveedu, S. Bhattacharya, *Chem. Asian J*. **2017**, 12, 76–85
50. N. Dey, S. K. Samanta, S. Bhattacharya, *Chem. Commun.* **2017**, 53, 1486-1489
51. N. A. Kratochwil, W. Huber, F. Müller, M. Kansy, P. R. Gerber, *Biochem. Pharmacol.* **2002**, *64*, 1355-1374.
52. S. Reja, I. A. Khan, V. Bhalla, M. Kumar, *Chem. Commun.* **2016,** *52*, 1182-1185.
53. Y. Y. Wu, W. T. Yu, T. C. Hou, T. K. Liu, C. L. Huang, I. C. Chen, K. T. Tan, *Chem .Commun*. **2014**, *50*, 11507-11510.
54. S. S. Maity, S. Samanta, S.; Saha, P. Sardar, A. Pal, S. Dasgupta, S. Ghosh, *J. Chem. Phys,* 2008, **354**, 162-173.
55. G. Dey, P. Gaur, R. Giri, S. Ghosh, *Chem. Commun.* **2016**, *52*, 1887-1890.
56. H. Kumar, V. Devaraji, R. Joshi, M. K. Jadhao, P. Ahirkar, R. Prasath, P. Bhavana, S. K. Ghosh, *RSC Adv*. **2015**, *5*, 65496-65513.
57. J. Tang, F. Luan, X. Chen, *Bioorg Med Chem.* **2006**, *14*, 3210-3217.
58. Y. Wang, Y. Ni, *Analyst* **2014**, *139*, 416-424.
59. W. Zhang, P. Zhang, S. Zhang, C. Zhu, *Anal. Methods* **2014**, *6*, 2499-2505.
60. W. Liu, H. Li, Y. Wei, C. A. Dong, *RSC Adv.* **2017**, *7*, 26930-26934.
61. S. Huang, F. Li, C. Liao, B. Zheng, J. Du, D. Xiao, *Talanta* **2017**, *170*, 562-568.
62. H. Zhang, L. Yao, X. Yu, Y. Zhao, A. Fan, *Anal. Methods* **2015**, *7*, 9949-9956.
63. T. Peters, All About Albumin: Biochemistry, Genetics, and Medical Applications, Academic Press, San Diego, CA, **1996**.
64. S. Choi, E. Y. Choi, D. J. Kim, J. H. Kim, T. S. Kim, S. W. Oh, *Clin. Chim. Acta* **2004**, *339*, 147-156.
65. R. E. Wang, L. Tian, Y. H. A. Chang, *J Pharm Biomed Anal.* **2012**, *63*, 165.
66. S. Arques, P. J. Ambrosi, *Card. Failure,* **2011**, *17*, 451-458.
67. G. Fanali, A. D. Masi, V. Trezza, M. Marino, M. Fasano, P. Ascenzi, *Mol. Aspects Med*. **2012**, *33*, 209.

68. K. T. Izutsu, E. L. Truelove, W. A. Bleyer, W. M. Anderson, M. M. Schubert, J. C. Rice, *Cancer* **1981**, *48*, 1450-1454.
69. B. Maji, K. Kumar, M. Kaulage, K. Muniyappa, S. Bhattacharya, *J Med Chem.* **2014**, *57*, 6973-6988
70. B. Maji, K. Kumar, K. Muniyappa, S. Bhattacharya, *Org Biomol Chem*. **2015**, *13*, 8335-8348.
71. L. Hu, S. Han, S. Parveen, Y. Yuan, L. Zhang, G. Xu, *Biosens. Bioelectron.* **2012**, *32*, 297-299.
72. J. P. Xu, Y. Fang, Z. G. Song, J. Mei, L. Jia, A. Qin, J. Z. Sun, J. Ji, B. Z. Tang, *Analyst* **2011**, *136*, 2315-2321.
73. X. Du, Y. Li, Y. L. Xia, S. M. Ai, J. Liang, P. Sang, X. L. Ji, S. Q. Liu, *Int. J. Mol. Sci.* **2016,** *17*, 144 (1-34).

Table of Contents

FULL PAPER

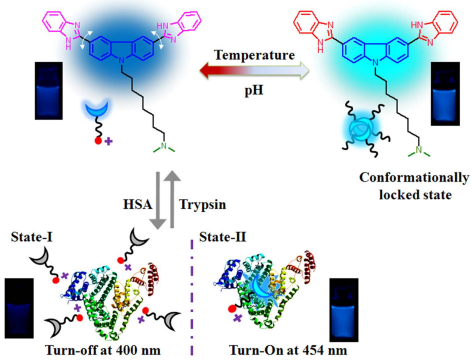

*Nilanjan Dey, Basudeb Maji and Santanu Bhattacharya**

Page No. – Page No.
Title: Motion Induced Change in Emission as an Effective Strategy for Ratiometric Probing of Human Serum Albumin and Trypsin in Biological Fluids